ORIGINAL PAPER

Structure and stability of kaolinite/TiO₂ nanocomposite: DFT and MM computations

Jonáš Tokarský · Pavla Čapková · Jaroslav V. Burda

Abstract The adhesion of TiO₂ (anatase structure) nanoparticles to kaolinite substrate was investigated using molecular modeling. Universal force field computation, density function theory computation, and a combination of both two approaches were used. This study enabled the adhesion energy for the TiO₂/kaolinite nanocomposite to be estimated, and revealed the preferred orientation of the TiO₂ nanoparticles on the kaolinite substrate. The results of all three levels of computation were compared in order to show that the accuracy of universal force field computations is sufficient in this context. The role of nanoparticle size and the importance of the nanoparticle–substrate bonding contribution are presented here and discussed. A comparison of the molecular modeling results with scanning electron microscopy observations showed that the results of the modeling were consistent with the experimental data, and that this approach can be used to help characterize nanocomposites of the nanoparticle/phyllosilicate substrate type.

Keywords Molecular modeling · TiO₂ · Kaolinite · DFT calculations · Surface interactions

J. Tokarský (✉) · P. Čapková
Nanotechnology Centre, VŠB-Technical University of Ostrava,
17. listopadu 15/2172,
708 33 Ostrava-Poruba, Czech Republic
e-mail: jonas.tokarsky@vsb.cz

J. V. Burda
Department of Chemical Physics and Optics,
Faculty of Mathematics and Physics, Charles University,
Ke Karlovu 3,
121 16 Prague, Czech Republic

Introduction

Titanium dioxide (TiO₂) is a widely studied semiconductor with a great number of practical applications due to not only its high refractive index and therefore high whiteness (useful in the cosmetic industry [1] and for paper coating [2]) but also (indeed mainly) its photocatalytic activity. Among the three crystallographic modifications of the TiO₂ structure: rutile, brookite, and anatase, the latter exhibits the highest photocatalytic activity and is therefore the most frequently studied, especially in relation to the photodegradation of environmental pollutants [3–5].

The surface and structural properties of TiO₂ as well as many other examples of its practical applications can be found in [6], while the photodegradation mechanism of TiO₂ is summarized, for example, in [7] and [8].
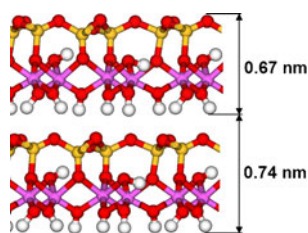
In spite of the fact that TiO₂ is currently regarded as a nontoxic material [9, 10], the possibility that it is a biohazard has still not been ruled out [11]. Therefore, materials containing TiO₂ nanoparticles pose a threat due to the danger of releasing nanoparticles into the environment [12, 13]. Since the question of its toxicity remains open, the release of TiO₂ nanoparticles from materials into the environment must be restrained. The simplest way to do this is to grow the TiO₂ nanoparticles on the surface of a suitable substrate and anchor them to it. Anchoring TiO₂ nanoparticles to a crystalline substrate also allows easy manipulation (it is very difficult to manipulate single nanoparticles).

Kaolinite (KLT), which belongs to the serpentinite–kaolinite group, is a dioctahedral phyllosilicate of 1:1 layer type. This phyllosilicate contains only a negligible amount of substitutions. It is a cheap and abundant natural material that represents (due to its unique crystallochemical properties) an excellent substrate for anchoring metal oxide nanoparticles [14, 15]. The structure of KLT can be seen in Fig. 1.

Fig. 1 A side view of the KLT structure, including the thickness of the layer and the basal spacing. *Beige* Si, *pink* Al, *red* O, *white* H (note that the web version of this article contains the color version of this figure)

Nanocomposite TiO_2/KLT is a material that combines properties of both of its components. The nanoparticles anchored on the KLT substrate retain their photoactivity and do not endanger either the environment or human health. Moreover, manipulating the TiO_2/KLT nanocomposite is much easier than manipulating pure TiO_2 nanoparticles, so the separation of TiO_2/KLT can be accomplished by filtration or (in the case of bigger KLT particles) by sedimentation.

Various methods of preparing TiO_2/KLT have been reported, including the use of $TiCl_4$ [16–18] or Ti(IV) alkoxides—i.e., Ti(IV) propoxide [19] or Ti(IV) butoxide [14, 20]—as precursors. Moreover, chemical or thermal pretreatment of KLT is commonly used [14, 16, 17, 20]. In the experimental part of our work, we prepared TiO_2/KLT using KLT in the as-received state and the very efficient and cheap precursor $TiOSO_4$ [21, 22].

The research presented in this report focused on the molecular modeling of the KLT/TiO_2 nanocomposite. Molecular mechanics and DFT computations were chosen for this purpose. While DFT computations on the structure and energetics of stoichiometric anatase surfaces as well as the formation energies of the most common orientations of the anatase have been performed by Lazzeri et al. [23, 24], to our knowledge no DFT computational results that have focused directly on the structure and stability of the KLT/TiO_2 nanocomposite have been published. Molecular modeling using the universal force field has proven to be a useful tool when investigating the structure and stability of nanoparticle/clay nanocomposites [25, 26]. Our first aim was to compare the results of DFT computations with those of universal force field computations in order to show that universal force field computations are sufficiently accurate for our purposes, and that the results obtained from them are similar to those gained from the DFT calculations.

Our second aim was to predict the structure (by searching for the best mutual crystallographic orientation of TiO_2 and KLT) and stability (by computing the adhesion energy between the TiO_2 nanoparticles and the KLT substrate) in order to complement the information obtained by experimental analyses of real samples of the KLT/TiO_2 nanocomposite described in our recent paper [21].

Strategy for modeling

Modeling conditions of empirical force field computations

Molecular modeling with the universal force field (UFF) [27] as implemented in the Accelrys Materials Studio modeling environment was used to study the adhesion forces between the TiO_2 nanoparticles and KLT substrate. Considering that Ti^{4+} is present in our models, we could not use any of following force fields: consistent-valence force field [28], Teppen force field [29, 30], CLAY force field [31], Morse charge equilibration force field [32], or the Dreiding force field [33].

Atomic charges were calculated by the QEq (charge equilibration) method [34], which has been shown to be suitable for clay-based nanocomposites [35–38].

The Smart algorithm (i.e., a cascade of the steepest descent, conjugate gradient, and quasi-Newton optimization algorithms) was used, with 50,000 iteration steps. Convergence criteria were 1×10^{-4} kcal for the energy and 5×10^{-5} Å for the displacement. The optimization of the initial models using UFF is denoted as "UFF opt." below.

Modeling conditions for DFT computations

In order to (at least roughly) estimate the error in the calculated interaction energies between the adsorbed nanoparticles and the surface of the KLT substrate, several model calculations were performed at the DFT level. For this purpose, HF/Lan2DZ [39, 40] optimizations were performed with single-point (SP) calculations of interaction (adhesion) energies at the DFT(B3LYP) [41, 42] level using the same basis set. Only interparticle distances and the mutual orientation of the TiO_2 nanoparticle with respect to the surface were optimized. The Gaussian G09 program [43] was used for these calculations. The optimization of the inital models using DFT is denoted "DFT opt." below, while the SP adhesion energy evaluation for the models optimized using molecular mechanics with the universal force field is denoted "DFT/UFF opt." These energies were determined to estimate the coordination covalent contributions, which are not known when the nanoparticle and substrate are in close proximity.

### Preparation of the models for empirical force field computations

M1 models

The structure of "real" KLT, i.e., $(Al_{7.8}Fe_{0.16}{}^{3+}K_{0.04})(Si_8)O_{20}(OH)_{16}$, was approximated by $(Al_8)(Si_8)O_{20}(OH)_{16}$. The KLT structure from [44] was used.

The first substrate (the tetrahedral surface of KLT) was built as a nonperiodic superstructure containing only the

tetrahedral sheet of KLT (i.e., aluminum atoms were omitted), as shown in Fig. 2a. The tetrahedral sheet contained six Si–O rings, and the overall formula of this substrate was $Si_{22}O_{61}H_{34}$. This idealized model with no cationic substitutions had a total layer charge of zero. The size was 2.2 nm×1.5 nm; thickness∼0.5 nm.

The second substrate (the octahedral surface of KLT) was built as a nonperiodic superstructure containing only the octahedral sheet of KLT (i.e., silicon atoms were omitted), as shown in Fig. 2b. This octahedral sheet consisted of six Al–O rings, and the overall formula of this
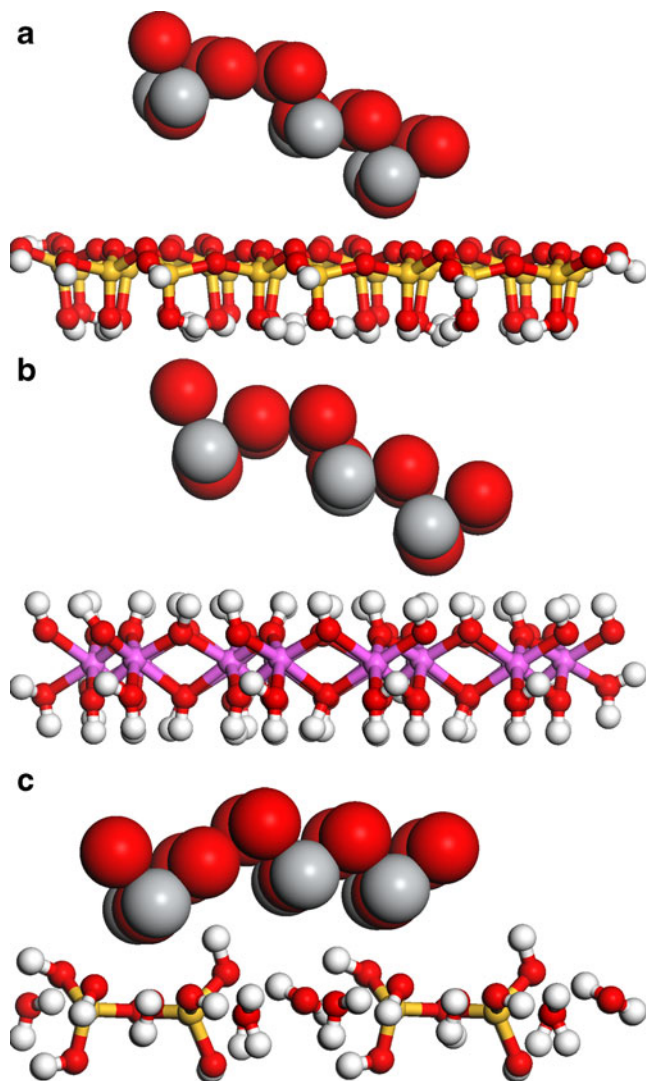
Fig. 2 **a** Optimized M1 model of $TiO_2(103)$ nanoparticle anchored to the tetrahedral basal surface of the kaolinite [i.e., KLT(001)Si]. *Gray* Ti, *red* O, *white* H, *beige* Si. **b** Optimized M1 model of the $TiO_2(103)$ nanoparticle anchored to the octahedral basal surface of the kaolinite [i.e., KLT(001)OH]. *Gray* Ti, *red* O, *white* H, *pink* Al. **c** Optimized M1 model containing a $TiO_2(103)$ nanoparticle anchored to the kaolinite edge [i.e., KLT(100)]. *Gray* Ti, *red* O, *white* H, *beige* Si. (Note that the web version of this article contains the color version of this figure)

substrate was $Al_{16}O_{58}H_{68}$. This idealized model with no cationic substitutions had a total layer charge of zero. The size was 1.9 nm×1.2 nm; thickness∼0.5 nm.

The third substrate (the edge of the KLT) was built as a nonperiodic superstructure containing fragments of three edges of three KLT layers (see Fig. 2c). Only the tetrahedral sheet of KLT was taken into account (i.e., Al atoms were omitted), so the overall formula of the prepared substrate was $Si_8O_{43}H_{54}$. This idealized model with no cationic substitutions had a total layer charge of zero. The size was 1.5 nm×1.8 nm; thickness∼0.25 nm.

Six TiO_2 nanoparticles (anatase structure [45]) with crystallographic orientations of (001), (100), (103), (110), and (112) and zero charge were prepared. The formulae of the nanoparticle were Ti_6O_{12} in the cases of $TiO_2(001)$, $TiO_2(103)$, $TiO_2(112)$; Ti_5O_{10} in the case of $TiO_2(100)$; and Ti_4O_8 in the case of $TiO_2(110)$. Because the distributions of atoms in the various hkl planes differed, each nanoparticle had a different adjacent surface size (see Table 1).

The prepared structures of the TiO_2 nanoparticles and KLT substrates were identical to those of the M1 models mentioned in the section "Preparation of M1 models for DFT computations" below; i.e., these models were used for UFF opt., DFT/UFF opt., and DFT opt. During the geometry optimization process, the substrates and TiO_2 nanoparticles were treated as rigid units, which means that the relative positions of the atoms inside each structure were fixed; the only motion allowed was that of the TiO_2 nanoparticle with respect to the KLT substrate.

M2 and M3 models

To obtain a model of reasonable size, the structure of "real" KLT, i.e., $(Al_{7.8}Fe_{0.16}{}^{3+}K_{0.04})(Si_8)O_{20}(OH)_{16}$, was approximated by $(Al_8)(Si_8)O_{20}(OH)_{16}$, as mentioned in the section

Table 1 The size of the adjacent surface of each TiO_2 nanoparticle and adhesion energies per $Å^2$ for the M1 models are listed in this table

TiO_2 nanoparticle on KLT	Size of adjacent surface ($Å^2$)	Adhesion energy (kcal/mol/$Å^2$)		
		DFT opt.	DFT/UFF opt.	UFF opt.
M_001	91.24	−0.50[a]	−0.31	−0.69
M_100	79.51	−1.50	−1.12	−0.81
M_103	68.85	−1.93[b]	−1.36	−1.07
M_110	107.38	−0.71	−0.29	−0.31
M_112	95.38	−1.55	−1.22	−1.04
Ma_103_1	68.85	−0.73	−0.65	−0.50
Ma_103_2	68.85	−0.21	−0.15	−0.52

BSSE-corrected values are: [a] −0.26; [b] −1.57

"M1 models" above. The KLT structure from [44] was also used here.

The KLT substrate was built as a nonperiodic superstructure containing six layers with an overall formula of $(Al_{1254})(Si_{1296})O_{3156}(OH)_{2640}$. This idealized model without any tetrahedral cationic substitutions had a total layer charge of $-6e$, which was entirely due to the nonstoichiometry at the edges (the edges of phyllosilicate platelets are negatively charged [46]). This negative charge arises as a consequence of the attack of positively charged sites at the edges of KLT by the SO_4^{2-} counteranion during the preparation of the composite from the $TiOSO_4$ precursor [47]. This precursor was used to prepare the real KLT/TiO_2 nanocomposite [21].

The layer charge was compensated by the anchored TiO_2 nanoparticle. The size of the KLT substrate was 5.1×4.4 nm (i.e., large enough to ensure that the TiO_2 nanoparticle was unaffected by the KLT substrate margin); thickness~4.2 nm. Basal spacing $d_{001}=0.74$ nm in this model, as this corresponds to the value for the real structure [21].

Two sets of TiO_2 nanoparticles (anatase structure [45]) with crystallographic orientations of (001), (100), (103), (110), and (112) and a charge of $+6e$ were prepared. The formula of each nanoparticle in the first set was $Ti_{39}O_{75}$ (models containing these smaller nanoparticles were denoted M2 models), while the formula of each nanoparticle in the second set was $Ti_{78}O_{153}$ (models containing these larger nanoparticles were denoted M3 models). The nanoparticles from each set were anchored on the same KLT substrate. Therefore, models M2 and M3 contained TiO_2 nanoparticles with two different sizes, but the KLT substrate was the same in both sets of models. In order to obtain more realistic results, the TiO_2 nanoparticles in both the M2 and the M3 models were treated during the UFF opt. without constraints. Because of the size of the models, DFT opt. and DFT/UFF opt. (which are much more time-consuming) were not used.

To enable comparison, the TiO_2 nanoparticles within each set complied with two conditions: (i) there was always the same number of atoms in the whole nanoparticle (114 in the first set and 231 in the second one), and (ii) there was always the same number of atoms in the plane adjacent to the KLT layer (24 atoms in the case of $Ti_{39}O_{75}$ and 48 atoms in the case of $Ti_{78}O_{153}$). Because the distributions of the atoms in the various hkl planes were not the same, the second condition constrains each nanoparticle to have a different adjacent area (see Table 2).

The initial M2 and M3 models were prepared by anchoring each nanoparticle to one of the three possible sites on the KLT substrate: tetrahedral surface [basal SiO surface, denoted KLT(001)Si; see Fig. 3a], octahedral surface [basal OH surface, denoted KLT(001)OH; see Fig. 3b], and the edge [denoted KLT(100); see Fig. 3c].

Preparation of M1 models for DFT computations

Since the number of electrons is a crucial limitation of DFT models, we had to restrict our models to systems with only several TiO_2 molecules (usually 4–6 neutral oxides) and a fixed shape (see the models discussed in the section "M1 models" above). Five TiO_2 crystallographic planes were considered: (001), (100), (103), (110), and (112). These TiO_2 nanoparticles interacted with relatively large surface areas of the KLT model (see "M1 models"). The models used for the DFT opt. were denoted M_001, M_100, M_103, M_110, M_112, Ma_103_1, and Ma_103_2 (see Table 1). The Ma_103_1 model contained the TiO_2(103) nanoparticle anchored to the tetrahedral surface of KLT; in the Ma_103_2 model, the TiO_2(103) nanoparticle is anchored to the octahedral surface of KLT [allowing a comparison of the TiO_2(103) model with all three "surfaces" from Fig. 2a].

The surface reactivity presented a delicate problem. We had to keep the conditions for the valence electrons from the surface layer as consistent as possible. Therefore, atoms from the second and partially also from the third layer were taken into account, to ensure that no artificial interaction types were included. In this way, the surface model always contained more than 100 atoms. The geometry of these atoms remained frozen in all calculations, and similarly the structure of TiO_2 particle was kept fixed, as only marginal geometry changes can occur in a larger structure due to the neighboring atoms in the solid nanoparticle. Since the size and especially the surface of the TiO_2 particle varied with the model used, all of the interaction energies obtained in our calculations were normalized to unit surface area ($1 \, Å^2$). All of the system geometries used (in x, y, z coordinates) are available upon request.

Computation of the adhesion energy

The interactions between the TiO_2 nanoparticles and the KLT substrates were quantified using the adhesion energy (E_{ad}):

$$E_{ad} = \frac{E_{tot} - (E_{tot,TiO2} + E_{tot,KLT})}{S}, \qquad (1)$$

where E_{tot} is the total energy of the nanocomposite (i.e., the TiO_2 nanoparticle anchored to the KLT substrate). $E_{tot, TiO2}$ is the total energy of the TiO_2 nanoparticle, $E_{tot, KLT}$ is the total energy of the KLT substrate, and S is the surface area of the TiO_2 nanoparticle adjacent to the KLT substrate. These energies were expressed in kcal mol^{-1} Å^{-2}.

Basis set superposition error (BSSE) was not considered in the DFT opt. and DFT/UFF opt. calculations due to the large size of the whole cluster.

Table 2 The adjacent surface sizes of TiO$_2$ nanoparticles and adhesion energies per Å^2. The values for both sets of TiO$_2$ nanoparticles (i.e., M2-TiO$_2$ and M3-TiO$_2$) are shown with respect to all three types of KLT surfaces (i.e., basal tetrahedral surface of KLT, edge of KLT, and basal octahedral surface of KLT)

TiO$_2$ nanoparticles on KLT	M2 models				M3 models			
	Size of adjacent surface (Å^2)	Adhesion energy (kcal/mol/Å^2)			Size of adjacent surface (Å^2)	Adhesion energy (kcal/mol/Å^2)		
		KLT(001) Si	KLT(001) OH	KLT(100)		KLT(001) Si	KLT(001) OH	KLT(100)
TiO$_2$(001)	152.6	−13.7	−17.6	−29.4	306.9	−15.3	−20.0	−26.4
TiO$_2$(100)	131.1	−17.1	−19.1	−31.5	181.4	−30.0	−31.9	−46.0
TiO$_2$(103)	172.9	−15.3	−24.8	−26.9	309.0	−17.6	−21.9	−23.9
TiO$_2$(110)	291.3	−4.3	−11.5	−14.4	546.2	−10.5	−15.4	−15.6
TiO$_2$(112)	142.7	−27.1	−30.4	−33.7	301.8	−23.8	−24.2	−19.9

Scanning electron microscopy (SEM) experiment

Nanocomposite KLT/TiO$_2$ particles were prepared in the following way. A suspension of nonpretreated KLT (SAK47; LB Minerals s.r.o., Horni Biiza, Czech Republic) and TiOSO$_4$ (Precheza a.s., Prerov, Czech Republic) was stirred for a while at laboratory temperature. In our typical experiment, 50 g of KLT were mixed with an appropriate volume of TiOSO$_4$ in order to obtain the desired amount of TiO$_2$ in the final composite. Then the suspension was heated to 95 °C and hydrolyzed by distilled water. After thermal hydrolysis, the resulting composite was washed several times with distilled water and dried at 105 °C overnight.

Scanning electron microscopy (SEM) was used to observe the prepared KLT/TiO$_2$ nanocomposite. The KLT substrate predominantly formed disc-shaped platelets of orientation (001), which were attached to the carbon surface of the sample holder. The samples of KLT with TiO$_2$ nanoparticles were coated with an Au/Pd film by chemical vapor deposition and observed using a Philips (Eindhoven, The Netherlands) XL30 scanning electron microscope. Images were obtained using a secondary-electron detector.

The preparation procedure and characterization methods used are described in detail in [21].

Results and discussion

M1 models: comparison of DFT and MM approaches

For the models optimized at the DFT level of computation (see "Preparation of M1 models for DFT computations"), the strongest adhesion energy E_{ad} was obtained for the TiO$_2$(103) nanoparticle (ca. −1.93 kcal mol^{-1} Å^{-2}), followed by the TiO$_2$(112) nanoparticle, leading to the order 103>112≈100>110>001. All values of E_{ad} normalized to 1 Å^2 are listed in Table 1, where the results of single-point (SP) energy evaluations for MM-optimized geometries (DFT/MM opt.) and the values predicted by molecular mechanics with UFF are also shown. Including the basis set superposition error (BSSE) would decrease the values of adhesion energy (we assume), but the differences between the individual systems with M1 models would be preserved, as follows from the results in Table 1.

We will now concentrate on comparing the adsorption on the two different planes of the substrate KLT (001) (i.e., tetrahedral and octahedral) with that on the KLT(100) plane (i.e., the edge). One can see that the models containing TiO$_2$ nanoparticles anchored to both the tetrahedral and octahedral planes of KLT(001) surfaces (i.e., models Ma_103_1 and Ma_103_2) exhibit lower E_{ad} values than the same model (M_103) of TiO$_2$ attached to the KLT(100) surface. Actually, their adhesion energies are also the lowest in reality. The same fact is also observed for all TiO$_2$ nanoparticles in the M2 and M3 models.

Our second comparison deals with the same substrate plane and various orientations of the interacting TiO$_2$ nanoparticle. Taking into account only the KLT(100)/TiO$_2$ models, listing them in descending order of E_{ad} allows us to compare the three following series. Only the Miller indices of the TiO$_2$ planes are used instead of the full notation of the models for the sake of simplicity.

$(103) > (112) \approx (100) > (110) > (001)$ M1_KLT(100)/TiO$_2$(DFT opt.)
$(103) > (112) \approx (100) > (001) \approx (110)$ M1_KLT(100)/TiO$_2$(DFT/UFF opt.)
$(103) \approx (112) > (001) \approx (100) > (110)$ M1_KLT(100)/TiO$_2$(UFF opt.)

The first motivation to perform DFT/UFF opt. calculations was the possibility of directly comparing the structures obtained by both the QM and the MM techniques at the same computational level. This allows us to investigate why the minima order changes with the level. From Table 1, it follows that all DFT/UFF values are visibly smaller (due to "optimal" relaxation of the DFT opt. models), which also
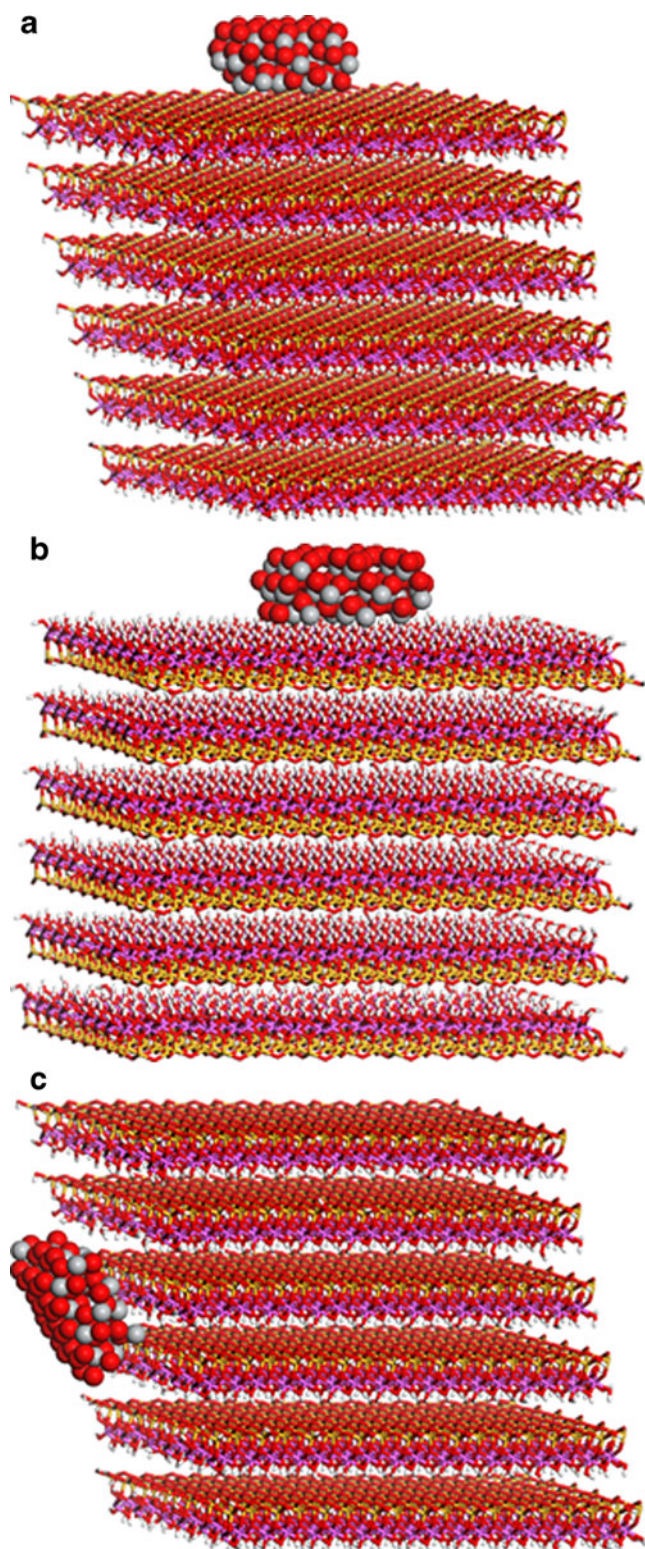
Fig. 3 a Optimized M2 model of a $TiO_2(112)$ nanoparticle anchored to the tetrahedral basal surface of kaolinite [i.e., KLT(001)Si]. **b** Optimized M2 model of a $TiO_2(112)$ nanoparticle anchored to the octahedral basal surface of kaolinite [i.e., KLT(001)OH]. **c** Optimized M2 model of a $TiO_2(112)$ nanoparticle anchored to the kaolinite edge [i.e., KLT(100)]. *Gray* Ti, *red* O, *white* H, *beige* Si, *pink* Al. (Note that the web version of this article contains the color version of this figure)

indicates the importance of covalent bonding between the nanoparticle and substrate. Such an interaction is not possible at the MM level. Based on this comparison, because the highest adhesion energy obtained at all three computational levels is the same, the covalent contributions in the (103), (112), and (110) models must be similar. This gives us a fair degree of confidence that the molecular modeling results are accurate. Only some small deviations for the adhesion energies of (001) systems are observed.

M2 and M3 models

Ahdesion energies E_{ad} per $Å^2$ for the optimized structures of the M2 and M3 models are listed in Table 2.

It is apparent that E_{ad} is significantly higher for models containing TiO_2 nanoparticles anchored to the KLT(100) edges, while it is lower for KLT(001)Si and KLT(001)OH substrates. The E_{ad} values for TiO_2 nanoparticles interacting with KLT(001)OH are slightly higher than those for TiO_2 nanoparticles anchored to KLT(001)Si. This is caused by the negative charge of the octahedra.

The M2 and M3 models can be ordered according to decreasing E_{ad} as follows:

(112) >	(100) >	(103) ≈	(001) >	(110)	M2_KLT(001)Si/TiO_2
(112) >	(103) >	(100) ≈	(001) >	(110)	M2_KLT(001)OH/TiO_2
(112) >	(100) >	(001) >	(103) >	(110)	M2_KLT(100)/TiO_2
(100) >	(112) >	(103) >	(001) >	(110)	M3_KLT(001)Si/TiO_2
(100) >	(112) >	(103) ≈	(001) >	(110)	M3_KLT(001)OH/TiO_2
(100) >	(001) >	(103) >	(112) >	(110)	M3_KLT(100)/TiO_2

Only a weak interaction is obtained for the model M3_KLT (100)/TiO_2(112): E_{ad} value is ca. -20 kcal mol^{-1} $Å^{-2}$, while the strongest interaction is predicted for the M2_KLT(100)/TiO_2(112) model (with $E_{ad} = -34$ kcal mol^{-1} $Å^{-2}$). A similar preference for the (112) plane of the nanoparticle can also be observed for the other two substrate planes in the M2 model (see Table 2). In the case of the M2_KLT(100)/TiO_2(112) system, a quite unusual relative orientation of the TiO_2(112) nanoparticle and the KLT(100) surface occurs that differs significantly from those of the other M2 models. While the TiO_2(001), TiO_2(100), TiO_2(103), and TiO_2(110) nanoparticles are oriented practically parallel with the KLT(100) surface, the TiO_2(112) nanoparticle is inclined at an angle of ca. 24° to the KLT(100) surface (see Fig. 4). This specific orientation leads to two titanium atoms from the TiO_2 nanoparticle being in the proximity of two oxygens from the KLT(100) surface. The distances between the Ti and O atoms [d(Ti–O)] are 2.1 and 2.4 Å, respectively. Despite the fact that no new chemical (coordination covalent) bonds can form within the MM, they are easily inferred to exist based on the distances between these atoms.
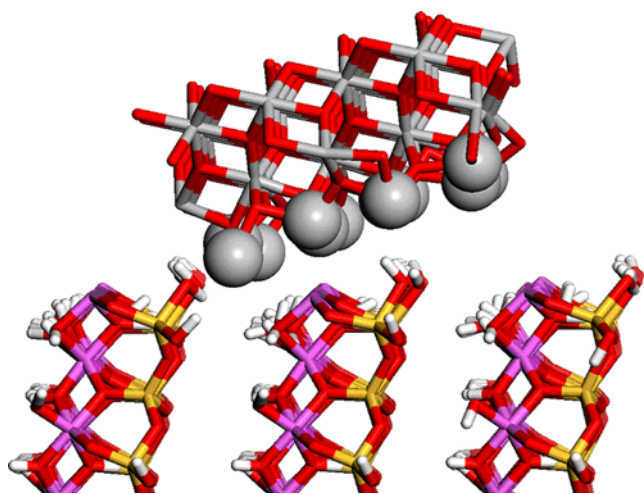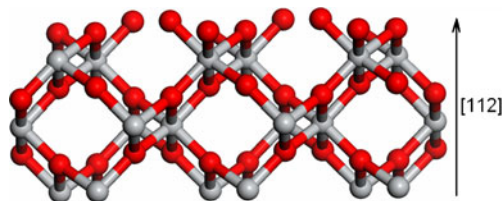
Fig. 4 TiO$_2$(112) nanoparticle in the model M2_KLT(100)/TiO$_2$(112). *Gray* Ti, *red* O, *white* H, *beige* Si, *pink* Al. (Note that the web version of this article contains the color version of this figure)

The average distance between the titanium atoms of the TiO$_2$ nanoparticle and the nearest oxygens of the KLT substrate in the other M2 models is larger than~2.8 Å. This shows that the M2_KLT(100)/TiO$_2$(112) model is exceptional.

There is another important difference between the TiO$_2$(112) cluster and the other nanoparticles. In contrast to the other modeled crystallographic planes of the TiO$_2$ anatase structure, there are no (112) planes in the [112] direction that contain both titanium and oxygen atoms; they each contain all titanium atoms or all oxygen atoms, as shown in Fig. 5.

If we place the M2 models in order of energy, practically the same preference for individual nanoparticles interacting with different substrate planes can be seen. The least favorite nanoparticle plane is (110).

For the M3 models, general agreement that the (100) nanoparticle provides the strongest adhesion is apparent. The larger (112) nanoparticle does not interact with the substrate as strongly, mainly due to the fact that specific

(local) interactions are not possible for these larger structures. In accord with the M2 model, the (110) plane is the least preferable.

Comparison of the M1, M2, and M3 models

The adhesion energies of the various M1, M2, and M3 models in the interactions of TiO$_2$ nanoparticles with the surface of the KLT(100) substrate can be placed in the following order:

(103) > (112) ≈ (100) > (110) > (001)   M1_KLT(100)/TiO$_2$(DFT opt.)
(103) > (112) ≈ (100) > (001) ≈ (110)   M1_KLT(100)/TiO$_2$(DFT/UFF opt.)
(103) ≈ (112) > (001) ≈ (100) > (110)   M1_KLT(100)/TiO$_2$(UFF opt.)
(112) > (100) > (001) > (103) > (110)   M2_KLT(100)/TiO$_2$
(100) > (001) > (103) > (112) > (110)   M3_KLT(100)/TiO$_2$

Some differences between the smallest M1 and the larger M2 models can be explained by the fact that the structure of the TiO$_2$ nanoparticle in the M2 (and M3) models is not fixed during the optimization process. The fixed positions of all atoms in the smallest M1 model are enforced by its structural simplicity.

Based on the order of adhesion energies for the M2 and M3 models, it is clear that the preferred orientation of the TiO$_2$ nanoparticles changes when larger TiO$_2$ nanoparticles are formed. As already mentioned above, taking into account the structural differences between the optimized M2 and M3 models, it can be stated that the size of the TiO$_2$ nanoparticle plays a significant role in its orientation with respect to the KLT substrate. While the smaller nanoparticles in the M2 models (and analogously also in the M1 models) can adopt various positions with respect to the KLT surface (i.e., they do not have to align parallel with the plane of the KLT substrate), the bigger nanoparticles in the M3 models are much more constrained in terms of their motion due to their size and the resulting larger adjacent surface. Moreover, they are also more rigid due to the larger covalently bonded neighborhood.

M2 and M3 models: substrates and nanoparticles with zero charges

In order to compare the values of E_{ad} for neutral and charged M2 and M3 models, the KLT substrate plus TiO$_2$(112) nanoparticle system was modified such that the KLT substrate was neutralized to the overall formula of (Al$_{1254}$)(Si$_{1296}$)O$_{3150}$(OH)$_{2646}$ with zero layer charge. The TiO$_2$(112) nanoparticles were modified in a similar manner. While the total number of atoms remained the same, the stoichiometric ratio changed from Ti$_{39}$O$_{75}$ to Ti$_{38}$O$_{76}$ in the M2 model, and similarly from Ti$_{78}$O$_{153}$ to Ti$_{77}$O$_{154}$ in the M3 model.

Fig. 5 Side view of the TiO$_2$(112) nanoparticle. The titanium atoms adjacent to the kaolinite substrate are shown at the bottom. It is apparent that each atomic layer in the [112] direction contains either oxygen or titanium atoms, but not a mixture of both. *Gray* Ti, *red* O. (Note that the web version of this article contains the color version of this figure)

Comparing values of E_{ad} in Table 2 and Table 3, it is clear that the electroneutral model does not match with experimental SEM observations, which indicated that TiO_2 nanoparticles are preferentially anchored to KLT edges (see Fig. 6). Such a structural arrangement of the TiO_2/KLT nanocomposite was also observed by Kočí et al. [22]. That group used the $TiOSO_4$ precursor and KLT in the as-received state, just as we did [21].
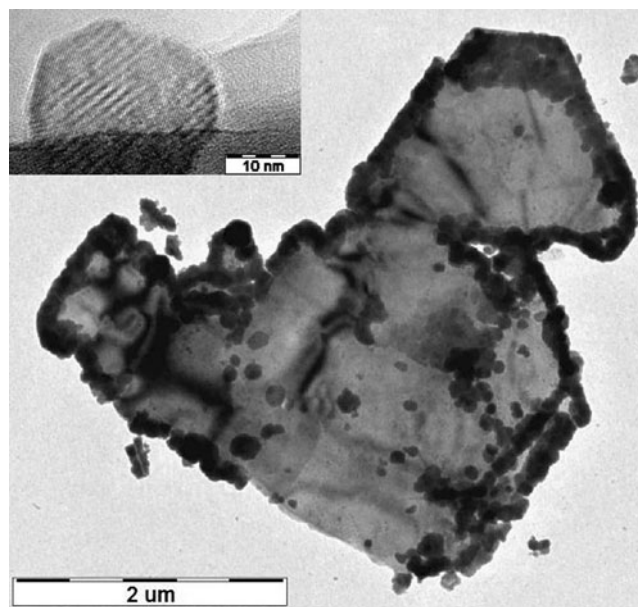
Nevertheless, another observation was made by Chong et al. and Vimonses et al., who published works describing the preparation of a TiO_2/KLT nanocomposite with a more or less uniform distribution of TiO_2 nanoparticles on the KLT substrate [14, 20]. However, they used another preparation method. In both works, a Ti(IV) butoxide precursor was used instead of $TiOSO_4$. Moreover, Chong et al. pretreated the pure KLT with NaOH (the resulting pH of the supernatant was 10) [20] and calcined the KLT at 750 °C. Vimonses et al. performed a series of acid (H_2SO_4)/ alkaline (NaOH)/thermal (calcination at 750 °C) treatments to alter the surface properties of the KLT [14]. Taking into account that the dehydroxylation of KLT to the metakaolinite phase occurs in the temperature range 450–700 °C [48–50], we are actually dealing with a different type of material in these two works [14, 20].

In the case of KLT(100), E_{ad} was weaker than those for both KLT(001)Si and KLT(001)OH. The E_{ad} values for KLT(100) are about one-third lower than the corresponding values for charged systems, clearly demonstrating the role of the additional electrostatic contribution. The original charged setting for molecular modeling follows from the known experimental constitutions of the samples. Nevertheless, the average change in the adhesion energy on both the KLT(001)Si and KLT(001)OH surfaces is only about 6% different from that for charged KLT(100) planes (cf. Table 2 and Table 3).

This shows that a substantial difference (a reduction of about 8 kcal mol^{-1} $Å^{-2}$) only occurs for the M2 and M3 models in the interaction of TiO_2 nanoparticles with the KLT(100) surface. Taking into account the method actually

Fig. 6 SEM micrograph of clusters of TiO_2 nanoparticles (*dark clusters*) growing on the edges [KLT(100)] of a kaolinite particle. A single TiO_2 nanoparticle can be seen in the *upper left corner*

used to prepare TiO_2/KLT nanocomposites [21], and the SEM observations of the final samples, we can state that the neutral models do not correspond to reality.

Conclusions

In this study, the results of molecular modeling were compared with those of ab initio calculations for small M1 models. Acceptable correspondence in terms of the preference for various planes of TiO_2 nanoparticles on the KLT substrate was obtained.

In accord with experimentally observed SEM results, the TiO_2 nanoparticles in all (M1, M2, M3) sets of models explored exhibited a tendency to adhere to the KLT(100) surface (i.e., the KLT edge).

Comparing the M2 and M3 models, the lower flexibility of the larger TiO_2 nanoparticles in the set of M3 models led to significantly lower adhesion to the KLT surface.

All three sets of models treated in this work predicted larger adhesion energies at the KLT(001)OH surface than at the KLT(001)Si surface.

Because new bond formation is not allowed in molecular modeling using an empirical force field, we used the adhesion energy and measured the distances between atoms instead. The fact that covalent bonds were only formed during the DFT computation in the models that had the highest adhesion energies (when treated by UFF) shows that these two approaches are in good agreement.

Table 3 The adjacent surface sizes of stoichiometric TiO_2 nanoparticles and adhesion energies per $Å^2$. These values are provided for both TiO_2(112) nanoparticles [i.e., M2-TiO_2(112) and M3-TiO_2(112)] and for all three types of KLT surface (i.e., basal tetrahedral surface of KLT, edge of KLT, and basal octahedral surface of KLT). The KLT substrate has zero layer charge

TiO_2 nanoparticles on KLT	Size of adjacent surface ($Å^2$)	Adhesion energy (kcal/mol/$Å^2$)		
		KLT(001) Si	KLT(001) OH	KLT (100)
M2_TiO_2(112)	142.68	−24.80	−31.96	−21.99
M3_TiO_2(112)	301.82	−25.48	−25.74	−14.80

References

1. Kertész Z, Szikszai Z, Gontier E, Moretto P, Surléve-Bazeille JE, Kiss B, Juhász I, Hunyadi J, Kiss AZ (2005) Nuclear microprobe study of TiO_2-penetration in the epidermis of human skin xenografts. Nucl Instrum Methods B 231:280–285

2. Park JK, Kim JK, Kim HK (2007) TiO_2-SiO_2 composite filler for thin paper. J Mater Process Technol 186:367–369

3. Dai K, Chen H, Peng T, Ke D, Yi H (2007) Photocatalytic degradation of methyl orange in aqueous suspension of mesoporous titania nanoparticles. Chemosphere 69:1361–1367

4. Zhang W, Zou L, Wang L (2009) Photocatalytic TiO_2/adsorbent nanocomposites prepared via wet chemical impregnation for wastewater treatment: a review. Appl Catal A 371:1–9

5. Ramirez AM, Demeestere K, De Belie N, Mantyla T, Levanen E (2010) Titanium dioxide coated cementitious materials for air purifying purposes: preparation, characterization and toluene removal potential. Build Environ 45:832–838

6. Diebold U (2003) The surface science of titanium dioxide. Surf Sci Rep 48:53–229

7. Fujishima A, Zhang X, Tryk DA (2008) TiO_2 photocatalysis and related surface phenomena. Surf Sci Rep 63:515–582

8. Carp O, Huisman CL, Reller A (2004) Photoinduced reactivity of titanium dioxide. Prog Solid State Chem 32:33–177

9. Warheit DB, Hoke RA, Finlay C, Maria Donner E, Reed KL, Sayes CM (2007) Development of a base set of toxicity tests using ultrafine TiO_2 particles as a component of nanoparticle risk management. Toxicol Lett 171:99–110

10. Jiang W, Mashayekhi H, Xing B (2009) Bacterial toxicity comparison between nano- and micro-scaled oxide particles. Environ Pollut 157:1619–1625

11. Li SQ, Zhu RR, Zhu H, Xue M, Sun XY, Yao SD, Wang SL (2008) Nanotoxicity of TiO_2 nanoparticles to erythrocyte in vitro. Food Chem Toxicol 46:3626–3631

12. Kaegi R, Ulrich A, Sinnet B, Vonbank R, Wichser A, Zuleeg S, Simmler H, Brunner S, Vonmont H, Burkhardt M, Boller M (2008) Synthetic TiO_2 nanoparticle emission from exterior facades into the aquatic environment. Environ Pollut 156:233–239

13. Reijnders L (2009) The release of TiO_2 and SiO_2 nanoparticles from nanocomposites. Polym Degrad Stab 94:873–876

14. Vimonses V, Chong MN, Jin B (2010) Evaluation of the physical properties and photodegradation ability of titania nanocrystalline impregnated onto modified kaolin. Microporous Mesoporous Mater 132:201–209

15. Szabó T, Németh J, Dékány I (2003) Zinc oxide nanoparticles incorporated in ultrathin layer silicate films and their photocatalytic properties. Colloids Surf A 230:23–35

16. Wang C, Shi H, Zhang P, Li Y (2011) Synthesis and characterization of kaolinite/TiO_2 nano-photocatalysts. Appl Clay Sci 53:646–649

17. Lu Z, Ren M, Yin H, Wang A, Ge C, Zhang Y, Yu L, Jiang T (2009) Preparation of nanosized anatase TiO_2-coated kaolin composites and their pigmentary properties. Powder Technol 196:122–125

18. Zhang Y, Gan H, Zhang G (2011) A novel mixed-phase TiO_2/kaolinite composites and their photocatalytic activity for degradation of organic contaminants. Chem Eng J 172:936–943

19. Kibanova D, Trejo M, Destaillats H, Cervini-Silva J (2009) Synthesis of hectorite-TiO_2 and kaolinite-TiO_2 nanocomposites

20. Chong MN, Vimonses V, Lei S, Jin B, Chow C, Saint C (2009) Synthesis and characterisation of novel titania impregnated kaolinite nano-photocatalyst. Microporous Mesoporous Mater 117:233–242

21. Mamulová Kutláková M, Tokarský J, Kovář P, Vojtěšková S, Kovářová A, Smetana B, Kukutschová J, Čapková P, Matějka V (2011) Preparation and characterization of photoactive composite kaolinite/TiO_2. J Hazard Mater 188:212–220

22. Kočí K, Matějka V, Kovář P, Lacný Z, Obalová L (2011) Comparison of the pure TiO_2 and kaolinite/TiO_2 composite as catalyst for CO_2 photocatalytic reduction. Catal Today 161:105–109

23. Lazzeri M, Vittadini A, Selloni A (2001) Structure and energetics of stoichiometric TiO_2 anatase surfaces. Phys Rev B 63:155409

24. Lazzeri M, Vittadini A, Selloni A (2002) Stress driven reconstruction of an oxide surface: the anatase $TiO_2(001)1×4$ surface. Phys Rev B 65:119901

25. Tokarský J, Čapková P, Rafaja D, Klemm V, Valášková M, Kukutschová J, Tomášek V (2010) Adhesion of silver nanoparticles on the clay substrates; modeling and experiment. Appl Surf Sci 256:2841–2848

26. Valášková M, Simha Martynková G, Lešková J, Čapková P, Klemm V, Rafaja D (2008) Silver nanoparticles/montmorillonite composites prepared using nitrating reagent at water and glycerol. J Nanosci Nanotechnol 8:3050–3058

27. Rappe AK, Casewit CJ, Colwell KS, Goddard WA, Skiff WM (1992) UFF, a full periodic table force field for molecular mechanics and molecular dynamics simulations. J Am Chem Soc 114:10024–10035

28. Kitson DH, Hagler AT (1988) Theoretical studies of the structure and molecular dynamics of a peptide crystal. Biochemistry 27:5246–5257

29. Teppen BJ, Rasmussen K, Bertsch PM, Miller DM, Schafer L (1997) Molecular dynamics modeling of clay minerals. 1. Gibbsite, kaolinite, pyrophyllite, and beidellite. J Phys Chem B 101:1579–1587

30. Teppen BJ, Yu CH, Newton SQ, Miller DM, Schäfer L (1998) Ab initio investigations pertaining to aluminum in tetrahedral octahedral sites of clay minerals. J Mol Struct 445:65–88

31. Cygan RT, Liang JJ, Kalinichev AG (2004) Molecular models of hydroxide, oxyhydroxide, and clay phases and the development of a general force field. J Phys Chem B 108:1255–1266

32. Hwang S, Blanco M, Demiralp E, Cagin T, Goddard WA (2001) The MS-Q force field for clay minerals: application to oil production. J Phys Chem B 105:4122–4127

33. Mayo SL, Olafson BD, Goddard WA (1990) DREIDING: a generic forcefield. J Phys Chem 94:8897–8909

34. Rappe AK, Goddard WA (1991) Charge equilibration for molecular dynamics simulations. J Phys Chem 95:3358–3363

35. Veteška M, Pospíšil M, Melánová K, Beneš L, Zima V (2008) Structure analysis of hydrotalcite intercalated with pyrenetetrasulfonate; experiments and molecular modelling. J Mol Model 14:1119–1129

36. Kovář P, Pospíšil M, Malý P, Klika Z, Čapková P, Horáková P, Valášková M (2009) Molecular modeling of surface modification of Wyoming and Cheto montmorillonite by methylene blue. J Mol Model 15:1391–1396

37. Kulhánková L, Čapková P, De Valle RV, Poyato J, Pérez-Rodríguez JL, Lerf A (2008) Surface and interlayer structure of vermiculite intercalated with methyl viologen. J Mol Model 14:1183–1189

38. Bongiovanni R, Mazza D, Ronchetti S, Turcato EA (2006) The influence of water on the intercalation of epoxy monomers in Na-montmorillonite. J Colloid Interface Sci 296:515–519

39. Hay PJ, Wadt WR (1985) Ab initio effective core potentials for molecular calculations. Potentials for K to Au including the outermost core orbitals. J Chem Phys 82:299–310

40. Hay PJ, Wadt WR (1985) Ab Initio effective core potentials for molecular calculations. Potentials for the transition metal atoms Sc to Hg. J Chem Phys 82:270–283

41. Becke AD (1988) Density-functional exchange-energy approximation with correct asymptotic behavior. Phys Rev A 38(6):3098–3100

42. Lee C, Yang W, Parr RG (1988) Development of the Colle–Salvetti correlation-energy formula into a functional of the electron density. Phys Rev B 37:785–789

43. Frisch MJ, Trucks GW, Schlegel HB, Scuseria GE, Robb MA, Cheeseman JR, Scalmani G, Barone V, Mennucci B, Petersson GA, Nakatsuji H, Caricato M, Li X, Hratchian HP, Izmaylov AF, Bloino J, Zheng G, Sonnenberg JL, Hada M, Ehara M, Toyota K, Fukuda R, Hasegawa J, Ishida M, Nakajima T, Honda Y, Kitao O, Nakai H, Vreven T, JMontgomery JA Jr., Peralta JE, Ogliaro F, Bearpark M, Heyd JJ, Brothers E, Kudin KN, Staroverov VN, Kobayashi R, Normand J, Raghavachari K, Rendell A, Burant JC, Iyengar SS, Tomasi J, Cossi M, Rega N, Millam JM, Klene M, Knox JE, Cross JB, Bakken V, Adamo C, Jaramillo J, Gomperts R, Stratmann RE, Yazyev O, Austin AJ, Cammi R, Pomelli C, Ochterski JW, Martin RL, Morokuma K, Zakrzewski VG, Voth GA, Salvador P, Dannenberg JJ, Dapprich S, Daniels AD, Farkas Ö, Foresman JB, Ortiz JV, Cioslowski J, Fox DJ (2009) Gaussian 09, revision A.1. Gaussian Inc., Wallingford

44. Neder RB, Burghammer M, Grasl T, Schulz H, Bram A, Fiedler S (1999) Refinement of the kaolinite structure from single-crystal synchrotron data. Clays Clay Miner 47:487–494

45. Howard CJ, Sabine TM, Dickson F (1991) Structural and thermal parameters for rutile and anatase. Acta Crystallogr B 47:462–468

46. Brady PV, Cygan RT, Nagy KL (1996) Molecular controls on kaolinite surface charge. J Colloid Interface Sci 183:356–364

47. Panda AK, Mishra BG, Mishra DK, Singh RK (2010) Effect of sulphuric acid treatment on the physico-chemical characteristics of kaolin clay. Colloids Surf A 363:98–104

48. Ptáček P, Kubátová D, Havlica J, Brandštetr J, Šoukal F, Opravil T (2010) Isothermal kinetic analysis of the thermal decomposition of kaolinite: the thermogravimetric study. Thermochim Acta 501:24–29

49. Konan KL, Peyratout C, Smith A, Bonnet JP, Rossignol SS, Oyetola S (2009) Comparison of surface properties between kaolin and metakaolin in concentrated lime solutions. J Colloid Interface Sci 339:103–109

50. Castellano M, Turturro A, Riani P, Montanari T, Finocchio E, Ramis G, Busca G (2010) Bulk and surface properties of commercial kaolins. Appl Clay Sci 48:446–454